

Observation of $e^+e^- \rightarrow \phi\chi_{c1}$ and $\phi\chi_{c2}$ at $\sqrt{s} = 4.600$ GeV

M. Ablikim¹, M. N. Achasov^{9,d}, S. Ahmed¹⁴, M. Albrecht⁴, A. Amoroso^{53A,53C}, F. F. An¹, Q. An^{50,40}, J. Z. Bai¹, Y. Bai³⁹, O. Bakina²⁴, R. Baldini Ferroli^{20A}, Y. Ban³², D. W. Bennett¹⁹, J. V. Bennett⁵, N. Berger²³, M. Bertani^{20A}, D. Bettoni^{21A}, J. M. Bian⁴⁷, F. Bianchi^{53A,53C}, E. Boger^{24,b}, I. Boyko²⁴, R. A. Briere⁵, H. Cai⁵⁵, X. Cai^{1,40}, O. Cakir^{43A}, A. Calcaterra^{20A}, G. F. Cao^{1,44}, S. A. Cetin^{43B}, J. Chai^{53C}, J. F. Chang^{1,40}, G. Chelkov^{24,b,c}, G. Chen¹, H. S. Chen^{1,44}, J. C. Chen¹, M. L. Chen^{1,40}, P. L. Chen⁵¹, S. J. Chen³⁰, X. R. Chen²⁷, Y. B. Chen^{1,40}, X. K. Chu³², G. Cibinetto^{21A}, H. L. Dai^{1,40}, J. P. Dai^{35,h}, A. Dbeyssi¹⁴, D. Dedovich²⁴, Z. Y. Deng¹, A. Denig²³, I. Denysenko²⁴, M. Destefanis^{53A,53C}, F. De Mori^{53A,53C}, Y. Ding²⁸, C. Dong³¹, J. Dong^{1,40}, L. Y. Dong^{1,44}, M. Y. Dong^{1,40,44}, Z. L. Dou³⁰, S. X. Du⁵⁷, P. F. Duan¹, J. Fang^{1,40}, S. S. Fang^{1,44}, Y. Fang¹, R. Farinelli^{21A,21B}, L. Fava^{53B,53C}, S. Fegan²³, F. Feldbauer²³, G. Felici^{20A}, C. Q. Feng^{50,40}, E. Fioravanti^{21A}, M. Fritsch^{23,14}, C. D. Fu¹, Q. Gao¹, X. L. Gao^{50,40}, Y. Gao⁴², Y. G. Gao⁶, Z. Gao^{50,40}, I. Garzia^{21A}, K. Goetzen¹⁰, L. Gong³¹, W. X. Gong^{1,40}, W. Gradl²³, M. Greco^{53A,53C}, M. H. Gu^{1,40}, Y. T. Gu¹², A. Q. Guo¹, R. P. Guo^{1,44}, Y. P. Guo²³, Z. Haddadi²⁶, S. Han⁵⁵, X. Q. Hao¹⁵, F. A. Harris⁴⁵, K. L. He^{1,44}, X. Q. He⁴⁹, F. H. Heinsius⁴, T. Held⁴, Y. K. Heng^{1,40,44}, T. Holtmann⁴, Z. L. Hou¹, H. M. Hu^{1,44}, T. Hu^{1,40,44}, Y. Hu¹, G. S. Huang^{50,40}, J. S. Huang¹⁵, X. T. Huang³⁴, X. Z. Huang³⁰, Z. L. Huang²⁸, T. Hussain⁵², W. Ikegami Andersson⁵⁴, Q. Ji¹, Q. P. Ji¹⁵, X. B. Ji^{1,44}, X. L. Ji^{1,40}, X. S. Jiang^{1,40,44}, X. Y. Jiang³¹, J. B. Jiao³⁴, Z. Jiao¹⁷, D. P. Jin^{1,40,44}, S. Jin^{1,44}, Y. Jin⁴⁶, T. Johansson⁵⁴, A. Julin⁴⁷, N. Kalantar-Nayestanaki²⁶, X. L. Kang¹, X. S. Kang³¹, M. Kavatsyuk²⁶, B. C. Ke⁵, T. Khan^{50,40}, A. Khoukaz⁴⁸, P. Kiese²³, R. Kliemt¹⁰, L. Koch²⁵, O. B. Kolcu^{43B,f}, B. Kopf⁴, M. Kornicer⁴⁵, M. Kuemmel⁴, M. Kuessner⁴, M. Kuhlmann⁴, A. Kupsc⁵⁴, W. Kühn²⁵, J. S. Lange²⁵, M. Lara¹⁹, P. Larin¹⁴, L. Lavezzi^{53C}, H. Leithoff²³, C. Leng^{53C}, C. Li⁵⁴, Cheng Li^{50,40}, D. M. Li⁵⁷, F. Li^{1,40}, F. Y. Li³², G. Li¹, H. B. Li^{1,44}, H. J. Li^{1,44}, J. C. Li¹, Jin Li³³, K. J. Li⁴¹, Kang Li¹³, Ke Li¹, Lei Li³, P. L. Li^{50,40}, P. R. Li^{44,7}, Q. Y. Li³⁴, W. D. Li^{1,44}, W. G. Li¹, X. L. Li³⁴, X. N. Li^{1,40}, X. Q. Li³¹, Z. B. Li⁴¹, H. Liang^{50,40}, Y. F. Liang³⁷, Y. T. Liang²⁵, G. R. Liao¹¹, D. X. Lin¹⁴, B. Liu^{35,h}, B. J. Liu¹, C. X. Liu¹, D. Liu^{50,40}, F. H. Liu³⁶, Fang Liu¹, Feng Liu⁶, H. B. Liu¹², H. M. Liu^{1,44}, Huanhuan Liu¹, Huihui Liu¹⁶, J. B. Liu^{50,40}, J. P. Liu⁵⁵, J. Y. Liu^{1,44}, K. Liu⁴², K. Y. Liu²⁸, Ke Liu⁶, L. D. Liu³², P. L. Liu^{1,40}, Q. Liu⁴⁴, S. B. Liu^{50,40}, X. Liu²⁷, Y. B. Liu³¹, Z. A. Liu^{1,40,44}, Zhiqing Liu²³, Y. F. Long³², X. C. Lou^{1,40,44}, H. J. Lu¹⁷, J. G. Lu^{1,40}, Y. Lu¹, Y. P. Lu^{1,40}, C. L. Luo²⁹, M. X. Luo⁵⁶, X. L. Luo^{1,40}, X. R. Lyu⁴⁴, F. C. Ma²⁸, H. L. Ma¹, L. L. Ma³⁴, M. M. Ma^{1,44}, Q. M. Ma¹, T. Ma¹, X. N. Ma³¹, X. Y. Ma^{1,40}, Y. M. Ma³⁴, F. E. Maas¹⁴, M. Maggiora^{53A,53C}, Q. A. Malik⁵², Y. J. Mao³², Z. P. Mao¹, S. Marcello^{53A,53C}, Z. X. Meng⁴⁶, J. G. Messchendorp²⁶, G. Mezzadri^{21B}, J. Min^{1,40}, T. J. Min¹, R. E. Mitchell¹⁹, X. H. Mo^{1,40,44}, Y. J. Mo⁶, C. Morales Morales¹⁴, N. Yu. Muchnoi^{9,d}, H. Muramatsu⁴⁷, P. Musiol⁴, A. Mustafa⁴, Y. Nefedov²⁴, F. Nerling¹⁰, I. B. Nikolaev^{9,d}, Z. Ning^{1,40}, S. Nisar⁸, S. L. Niu^{1,40}, X. Y. Niu^{1,44}, S. L. Olsen^{33,j}, Q. Ouyang^{1,40,44}, S. Pacetti^{20B}, Y. Pan^{50,40}, M. Papenbrock⁵⁴, P. Patteri^{20A}, M. Pelizaeus⁴, J. Pellegrino^{53A,53C}, H. P. Peng^{50,40}, K. Peters^{10,g}, J. Pettersson⁵⁴, J. L. Ping²⁹, R. G. Ping^{1,44}, A. Pitka²³, R. Poling⁴⁷, V. Prasad^{50,40}, H. R. Qi², M. Qi³⁰, S. Qian^{1,40}, C. F. Qiao⁴⁴, N. Qin⁵⁵, X. S. Qin⁴, Z. H. Qin^{1,40}, J. F. Qiu¹, K. H. Rashid^{52,i}, C. F. Redmer²³, M. Richter⁴, M. Ripka²³, M. Rolo^{53C}, G. Rong^{1,44}, Ch. Rosner¹⁴, A. Sarantsev^{24,e}, M. Savrié^{21B}, C. Schnier⁴, K. Schoenning⁵⁴, W. Shan³², M. Shao^{50,40}, C. P. Shen², P. X. Shen³¹, X. Y. Shen^{1,44}, H. Y. Sheng¹, J. J. Song³⁴, W. M. Song³⁴, X. Y. Song¹, S. Sosio^{53A,53C}, C. Sowa⁴, S. Spataro^{53A,53C}, G. X. Sun¹, J. F. Sun¹⁵, L. Sun⁵⁵, S. S. Sun^{1,44}, X. H. Sun¹, Y. J. Sun^{50,40}, Y. K. Sun^{50,40}, Y. Z. Sun¹, Z. J. Sun^{1,40}, Z. T. Sun¹⁹, C. J. Tang³⁷, G. Y. Tang¹, X. Tang¹, I. Tapan^{43C}, M. Tiemens²⁶, B. Tsednee²², I. Uman^{43D}, G. S. Varner⁴⁵, B. Wang¹, B. L. Wang⁴⁴, D. Wang³², D. Y. Wang³², Dan Wang⁴⁴, K. Wang^{1,40}, L. L. Wang¹, L. S. Wang¹, M. Wang³⁴, Meng Wang^{1,44}, P. Wang¹, P. L. Wang¹, W. P. Wang^{50,40}, X. F. Wang⁴², Y. Wang³⁸, Y. D. Wang¹⁴, Y. F. Wang^{1,40,44}, Y. Q. Wang²³, Z. Wang^{1,40}, Z. G. Wang^{1,40}, Z. Y. Wang¹, Zongyuan Wang^{1,44}, T. Weber²³, D. H. Wei¹¹, P. Weidenkaff²³, S. P. Wen¹, U. Wiedner⁴, M. Wolke⁵⁴, L. H. Wu¹, L. J. Wu^{1,44}, Z. Wu^{1,40}, L. Xia^{50,40}, Y. Xia¹⁸, D. Xiao¹, H. Xiao⁵¹, Y. J. Xiao^{1,44}, Z. J. Xiao²⁹, Y. G. Xie^{1,40}, Y. H. Xie⁶, X. A. Xiong^{1,44}, Q. L. Xiu^{1,40}, G. F. Xu¹, J. J. Xu^{1,44}, L. Xu¹, Q. J. Xu¹³, Q. N. Xu⁴⁴, X. P. Xu³⁸, L. Yan^{53A,53C}, W. B. Yan^{50,40}, W. C. Yan², Y. H. Yan¹⁸, H. J. Yang^{35,h}, H. X. Yang¹, L. Yang⁵⁵, Y. H. Yang³⁰, Y. X. Yang¹¹, M. Ye^{1,40}, M. H. Ye⁷, J. H. Yin¹, Z. Y. You⁴¹, B. X. Yu^{1,40,44}, C. X. Yu³¹, J. S. Yu²⁷, C. Z. Yuan^{1,44}, Y. Yuan¹, A. Yuncu^{43B,a}, A. A. Zafar⁵², Y. Zeng¹⁸, Z. Zeng^{50,40}, B. X. Zhang¹, B. Y. Zhang^{1,40}, C. C. Zhang¹, D. H. Zhang¹, H. H. Zhang⁴¹, H. Y. Zhang^{1,40}, J. Zhang^{1,44}, J. L. Zhang¹, J. Q. Zhang¹, J. W. Zhang^{1,40,44}, J. Y. Zhang¹, J. Z. Zhang^{1,44}, K. Zhang^{1,44}, L. Zhang⁴², S. Q. Zhang³¹, X. Y. Zhang³⁴, Y. H. Zhang^{1,40}, Y. T. Zhang^{50,40}, Yang Zhang¹, Yao Zhang¹, Yu Zhang⁴⁴, Z. H. Zhang⁶, Z. P. Zhang⁵⁰, Z. Y. Zhang⁵⁵, G. Zhao¹, J. W. Zhao^{1,40}, J. Y. Zhao^{1,44}, J. Z. Zhao^{1,40}, Lei Zhao^{50,40}, Ling Zhao¹, M. G. Zhao³¹, Q. Zhao¹, S. J. Zhao⁵⁷, T. C. Zhao¹, Y. B. Zhao^{1,40}, Z. G. Zhao^{50,40}, A. Zhemchugov^{24,b}, B. Zheng⁵¹, J. P. Zheng^{1,40}, W. J. Zheng³⁴, Y. H. Zheng⁴⁴, B. Zhong²⁹, L. Zhou^{1,40}, X. Zhou⁵⁵, X. K. Zhou^{50,40}, X. R. Zhou^{50,40}, X. Y. Zhou¹, Y. X. Zhou¹², J. Zhu³¹, J. Zhu⁴¹, K. Zhu¹, K. J. Zhu^{1,40,44}, S. Zhu¹, S. H. Zhu⁴⁹, X. L. Zhu⁴², Y. C. Zhu^{50,40}, Y. S. Zhu^{1,44}, Z. A. Zhu^{1,44}, J. Zhuang^{1,40}, B. S. Zou¹, J. H. Zou¹

(BESIII Collaboration)

- ¹ Institute of High Energy Physics, Beijing 100049, People's Republic of China
- ² Beihang University, Beijing 100191, People's Republic of China
- ³ Beijing Institute of Petrochemical Technology, Beijing 102617, People's Republic of China
- ⁴ Bochum Ruhr-University, D-44780 Bochum, Germany
- ⁵ Carnegie Mellon University, Pittsburgh, Pennsylvania 15213, USA
- ⁶ Central China Normal University, Wuhan 430079, People's Republic of China
- ⁷ China Center of Advanced Science and Technology, Beijing 100190, People's Republic of China
- ⁸ COMSATS Institute of Information Technology, Lahore, Defence Road, Off Raiwind Road, 54000 Lahore, Pakistan
- ⁹ G.I. Budker Institute of Nuclear Physics SB RAS (BINP), Novosibirsk 630090, Russia
- ¹⁰ GSI Helmholtzcentre for Heavy Ion Research GmbH, D-64291 Darmstadt, Germany
- ¹¹ Guangxi Normal University, Guilin 541004, People's Republic of China
- ¹² Guangxi University, Nanning 530004, People's Republic of China
- ¹³ Hangzhou Normal University, Hangzhou 310036, People's Republic of China
- ¹⁴ Helmholtz Institute Mainz, Johann-Joachim-Becher-Weg 45, D-55099 Mainz, Germany
- ¹⁵ Henan Normal University, Xinxiang 453007, People's Republic of China
- ¹⁶ Henan University of Science and Technology, Luoyang 471003, People's Republic of China
- ¹⁷ Huangshan College, Huangshan 245000, People's Republic of China
- ¹⁸ Hunan University, Changsha 410082, People's Republic of China
- ¹⁹ Indiana University, Bloomington, Indiana 47405, USA
- ²⁰ (A)INFN Laboratori Nazionali di Frascati, I-00044, Frascati, Italy; (B)INFN and University of Perugia, I-06100, Perugia, Italy
- ²¹ (A)INFN Sezione di Ferrara, I-44122, Ferrara, Italy; (B)University of Ferrara, I-44122, Ferrara, Italy
- ²² Institute of Physics and Technology, Peace Ave. 54B, Ulaanbaatar 13330, Mongolia
- ²³ Johannes Gutenberg University of Mainz, Johann-Joachim-Becher-Weg 45, D-55099 Mainz, Germany
- ²⁴ Joint Institute for Nuclear Research, 141980 Dubna, Moscow region, Russia
- ²⁵ Justus-Liebig-Universitaet Giessen, II. Physikalisches Institut, Heinrich-Buff-Ring 16, D-35392 Giessen, Germany
- ²⁶ KVI-CART, University of Groningen, NL-9747 AA Groningen, The Netherlands
- ²⁷ Lanzhou University, Lanzhou 730000, People's Republic of China
- ²⁸ Liaoning University, Shenyang 110036, People's Republic of China
- ²⁹ Nanjing Normal University, Nanjing 210023, People's Republic of China
- ³⁰ Nanjing University, Nanjing 210093, People's Republic of China
- ³¹ Nankai University, Tianjin 300071, People's Republic of China
- ³² Peking University, Beijing 100871, People's Republic of China
- ³³ Seoul National University, Seoul, 151-747 Korea
- ³⁴ Shandong University, Jinan 250100, People's Republic of China
- ³⁵ Shanghai Jiao Tong University, Shanghai 200240, People's Republic of China
- ³⁶ Shanxi University, Taiyuan 030006, People's Republic of China
- ³⁷ Sichuan University, Chengdu 610064, People's Republic of China
- ³⁸ Soochow University, Suzhou 215006, People's Republic of China
- ³⁹ Southeast University, Nanjing 211100, People's Republic of China
- ⁴⁰ State Key Laboratory of Particle Detection and Electronics, Beijing 100049, Hefei 230026, People's Republic of China
- ⁴¹ Sun Yat-Sen University, Guangzhou 510275, People's Republic of China
- ⁴² Tsinghua University, Beijing 100084, People's Republic of China
- ⁴³ (A)Ankara University, 06100 Tandogan, Ankara, Turkey; (B)Istanbul Bilgi University, 34060 Eyup, Istanbul, Turkey; (C)Uludag University, 16059 Bursa, Turkey; (D)Near East University, Nicosia, North Cyprus, Mersin 10, Turkey
- ⁴⁴ University of Chinese Academy of Sciences, Beijing 100049, People's Republic of China
- ⁴⁵ University of Hawaii, Honolulu, Hawaii 96822, USA
- ⁴⁶ University of Jinan, Jinan 250022, People's Republic of China
- ⁴⁷ University of Minnesota, Minneapolis, Minnesota 55455, USA
- ⁴⁸ University of Muenster, Wilhelm-Klemm-Str. 9, 48149 Muenster, Germany
- ⁴⁹ University of Science and Technology Liaoning, Anshan 114051, People's Republic of China
- ⁵⁰ University of Science and Technology of China, Hefei 230026, People's Republic of China
- ⁵¹ University of South China, Hengyang 421001, People's Republic of China

⁵² *University of the Punjab, Lahore-54590, Pakistan*

⁵³ (A)*University of Turin, I-10125, Turin, Italy*; (B)*University of Eastern Piedmont, I-15121, Alessandria, Italy*; (C)*INFN, I-10125, Turin, Italy*

⁵⁴ *Uppsala University, Box 516, SE-75120 Uppsala, Sweden*

⁵⁵ *Wuhan University, Wuhan 430072, People's Republic of China*

⁵⁶ *Zhejiang University, Hangzhou 310027, People's Republic of China*

⁵⁷ *Zhengzhou University, Zhengzhou 450001, People's Republic of China*

^a *Also at Bogazici University, 34342 Istanbul, Turkey*

^b *Also at the Moscow Institute of Physics and Technology, Moscow 141700, Russia*

^c *Also at the Functional Electronics Laboratory, Tomsk State University, Tomsk, 634050, Russia*

^d *Also at the Novosibirsk State University, Novosibirsk, 630090, Russia*

^e *Also at the NRC "Kurchatov Institute", PNPI, 188300, Gatchina, Russia*

^f *Also at Istanbul Arel University, 34295 Istanbul, Turkey*

^g *Also at Goethe University Frankfurt, 60323 Frankfurt am Main, Germany*

^h *Also at Key Laboratory for Particle Physics, Astrophysics and Cosmology, Ministry of Education; Shanghai Key Laboratory for Particle Physics and Cosmology; Institute of Nuclear and Particle Physics, Shanghai 200240, People's Republic of China*

ⁱ *Government College Women University, Sialkot - 51310. Punjab, Pakistan.*

^j *Currently at: Center for Underground Physics, Institute for Basic Science, Daejeon 34126, Korea*

Using a data sample collected with the BESIII detector operating at the BEPCII storage ring at a center-of-mass energy of $\sqrt{s} = 4.600$ GeV, we search for the production of $e^+e^- \rightarrow \phi\chi_{c0,1,2}$. A search is also performed for the charmonium-like state $X(4140)$ in the radiative transition $e^+e^- \rightarrow \gamma X(4140)$ with $X(4140)$ subsequently decaying into $\phi J/\psi$. The processes $e^+e^- \rightarrow \phi\chi_{c1}$ and $\phi\chi_{c2}$ are observed for the first time, each with a statistical significance of more than 10σ , and the Born cross sections are measured to be $(4.2^{+1.7}_{-1.0} \pm 0.3)$ pb and $(6.7^{+3.4}_{-1.7} \pm 0.5)$ pb, respectively, where the first uncertainties are statistical and the second systematic. No significant signals are observed for $e^+e^- \rightarrow \phi\chi_{c0}$ and $e^+e^- \rightarrow \gamma X(4140)$ and upper limits on the Born cross sections at 90% confidence level are provided at $\sqrt{s} = 4.600$ GeV.

PACS numbers: 14.40.Pq, 14.40.Rt, 13.66.Bc

I. INTRODUCTION

In recent years, many charmonium-like states have been observed experimentally, whose characters are different from the predictions of the charmonium states in the potential model. The $X(3872)$ was first observed by the Belle Collaboration in $B^\pm \rightarrow K^\pm \pi^+ \pi^- J/\psi$ [1] and was subsequently confirmed by several other experiments [2–5]. The vector states $X(4260)$, $X(4360)$, and $X(4660)$, sometimes called the $Y(4260)$, $Y(4360)$, and $Y(4660)$, were discovered by the *BABAR*, Belle, and CLEO Collaborations via their decays into low-mass charmonium states $\pi^+ \pi^- J/\psi$ or $\pi^+ \pi^- \psi(3686)$ [6–10]. Some charged charmonium-like states and their neutral partners, such as $Z_c(3900)$, $Z_c(3885)$, $Z_c(4020)$, $Z_c(4025)$, $Z_c(4200)$ have been also observed by several experiments [11–21]. There are many theoretical interpretations on the nature of these XYZ states, such as molecular, hybrid, or multi-quark states, threshold enhancements, or some other configurations [22]. However, the nature of these states is still unclear. Due to the richness of XYZ states above the open charm threshold, searching for new decay modes of these states and measuring their line shape precisely will provide helpful information to determine the properties of them.

The authors of Ref. [23] predicted a sizable coupling be-

tween the $X(4260)$ and the $\omega\chi_{c0}$ channel by considering the threshold effect of the $\omega\chi_{c0}$. The BESIII Collaboration measured the cross sections of $e^+e^- \rightarrow \omega\chi_{c0,1,2}$ at center-of-mass (c.m.) energies between 4.23 and 4.60 GeV and determined the mass of an intermediate resonance to be about $4226 \text{ MeV}/c^2$, assuming that the $\omega\chi_{c0}$ signals come from a single resonance [24, 25]. These resonant parameters are also inconsistent with those obtained by fitting a single resonance to the $\pi^+ \pi^- J/\psi$ cross section [6, 7]. Recently, BESIII Collaboration precisely measured the cross section of $e^+e^- \rightarrow \pi^+ \pi^- J/\psi$ in the relevant mass range and observed two resonant structures whose masses are determined to be 4224 and 4319 MeV/c^2 [26]. The mass of the first state is lower than that from *BABAR* and Belle measurements corresponding to the $X(4260)$. The fact that the parameters of the $X(4260)$ agree with the structure observed by BESIII Collaboration in $e^+e^- \rightarrow \omega\chi_{c0}$ suggests that the $X(4260)$ have multiple decay modes. Considering that ω and ϕ mesons have the same spin, parity, and isospin, $\omega\chi_{cJ}$ and $\phi\chi_{cJ}$ may have a similar production mechanism. Therefore, we study and measure the cross sections of $e^+e^- \rightarrow \phi\chi_{c0,1,2}$.

The $X(4140)$, sometimes called the $Y(4140)$, was first reported by the CDF experiment in the decay $B^+ \rightarrow \phi J/\psi K^+$ [27]. However, the existence of the $X(4140)$ was neither confirmed by the Belle [28] and *BABAR* [29] Collaborations in the same process, nor by Belle

Collaboration in two-photon production [28]. Recently, the CMS [30] and DØ [31] Collaborations reported the observation of the $X(4140)$ with resonant parameters being consistent with those of the CDF measurement. More recently, the LHCb Collaboration observed the $X(4140)$ with a statistical significance of 8.4σ using a data sample of $3 \text{ fb}^{-1} pp$ collision in the same process [32], using a full amplitude analysis. BESIII Collaboration has searched for the $X(4140)$ in the process $e^+e^- \rightarrow \gamma\phi J/\psi$ with data samples at c.m. energies $\sqrt{s} = 4.23, 4.26, \text{ and } 4.36 \text{ GeV}$ [33], but no obvious signal has been observed.

In this article, we present the results of a study of $e^+e^- \rightarrow \phi\chi_{c0,1,2}$ and a search for the $X(4140)$ in process $e^+e^- \rightarrow \gamma X(4140) \rightarrow \gamma\phi J/\psi$, based on an e^+e^- annihilation data sample collected with the BESIII detector [34] at $\sqrt{s} = 4.600 \text{ GeV}$. The c.m. energy of the data sample is determined with a precision of 0.8 MeV [35] using di-muon events. The integrated luminosity of the sample is measured using large-angle Bhabha scattering to be 567 pb^{-1} with a precision of 1.0% [36].

II. DETECTOR AND MONTE CARLO SAMPLES

The Beijing Spectrometer III (BESIII) detector, described in detail in Ref. [34], is a magnetic spectrometer operating at the Beijing Electron-Positron collider (BEPCII), which is a double-ring e^+e^- collider with a c.m. energy range from 2.0 to 4.6 GeV . The cylindrical core of the BESIII detector consists of a helium-based main drift chamber (MDC), a plastic scintillator time-of-flight (TOF) system, and a CsI(Tl) electromagnetic calorimeter (EMC) that are all enclosed in a superconducting solenoid magnet providing a 1.0 T magnetic field. The magnet is supported by an octagonal flux-return yoke with modules of resistive plate muon counters (MUC) interleaved with steel. The acceptance of the MDC for charged tracks is 93% of 4π solid angle. It provides a charged particle momentum resolution of 0.5% at $1.0 \text{ GeV}/c$ and ionization energy loss (dE/dx) measurements with resolution better than 6% . The time resolution of the TOF is 80 (110) ps for the barrel (end caps) and the EMC measures photon energy with a resolution of 2.5% (5%) at 1.0 GeV in the barrel (end caps). The MUC provides a position resolution of 2 cm and detects muon tracks with momenta higher than $0.5 \text{ GeV}/c$.

The optimization of event selection, determination of the detection efficiency and estimation of the backgrounds are performed using the GEANT4-based [37] Monte Carlo (MC) simulation software BOOST [38]. It includes the geometric and material description for the BESIII detector and a simulation of the detector response. Signal MC samples of $e^+e^- \rightarrow \phi\chi_{c0,1,2}$ and $e^+e^- \rightarrow \gamma X(4140) \rightarrow \gamma\phi J/\psi$ are generated at $\sqrt{s} = 4.600 \text{ GeV}$, where each sample contains 10^5 events. Both χ_{c1} and χ_{c2} states are reconstructed via $\chi_{c1,2} \rightarrow \gamma J/\psi$, $J/\psi \rightarrow \ell^+\ell^-$ ($\ell = e$ or μ), and ϕ via its decay to K^+K^- . For $e^+e^- \rightarrow \phi\chi_{c0}$, since the branching fraction of $\chi_{c0} \rightarrow \gamma J/\psi$, with $J/\psi \rightarrow \ell^+\ell^-$ is smaller than those of $\chi_{c0} \rightarrow \pi^+\pi^-$, K^+K^- , $\pi^+\pi^-\pi^+\pi^-$, and $K^+K^-\pi^+\pi^-$,

the χ_{c0} state is reconstructed with the latter four channels. Initial state radiation effects are simulated with KKMC [39], where the production cross sections are assumed to follow the line shape of the $X(4660)$ [10], modified by a phase space factor. Final state radiation effects associated with charged particles are handled with PHOTOS [40].

An ‘‘inclusive’’ MC sample is also generated with an integrated luminosity equivalent to that of the data sample. QED events, $e^+e^- \rightarrow e^+e^-$, $\mu^+\mu^-$, and $\gamma\gamma$, are generated with BABAYAGA [41]. The processes including an intermediate $D_{(s)}^{(*)}$ meson such as $e^+e^- \rightarrow D\bar{D}$, $D^*\bar{D}^*$, $D\bar{D}^* + c.c.$, $D_s^+D_s^-$, $D_s^+D_s^{*-} + c.c.$, and $D_s^{*+}D_s^{*-}$, the known charmonium production processes, and the process $e^+e^- \rightarrow \Lambda_c^+\bar{\Lambda}_c^-$ with all their known decays are generated using EVTGEN [42]. The unmeasured but possible decays associated to charmonium states are generated with LUNDCHARM [43] and other hadronic events are generated with PYTHIA [44].

III. $e^+e^- \rightarrow \phi\chi_{c1}$ AND $\phi\chi_{c2}$

A. Event Selection

The final states for $e^+e^- \rightarrow \phi\chi_{c1}$ and $\phi\chi_{c2}$ are $\gamma K^+K^-\ell^+\ell^-$. For each charged track in the MDC, the polar angle must satisfy $|\cos\theta| < 0.93$ and the point of closest approach to the e^+e^- interaction point must be within $\pm 10 \text{ cm}$ in the beam direction and within 1 cm in the plane perpendicular to the beam direction. We require that there are at least three candidate charged tracks in the final state. Leptons from J/ψ decays can be separated from other tracks kinematically, hence the two tracks with momenta greater than $1.0 \text{ GeV}/c$ and opposite charge are assumed to be leptons. The energy deposited in the EMC is used to separate electrons from muons. For muon candidates, the deposited energy is required to be less than 0.6 GeV , while for electron candidates it is required to be greater than 1.0 GeV . The momenta of the kaons are about $0.2 \text{ GeV}/c$ in the laboratory frame, and low momentum kaons affect the reconstruction efficiency significantly. To increase the efficiency, only one kaon is required to be reconstructed and pass the particle identification (PID) requirements. For each charged track with low momentum, the PID probability $Prob_i$ ($i = \pi, K$) of each particle hypothesis is calculated, combining the dE/dx and TOF information. Here we require $Prob_K > Prob_\pi$.

Photon candidates are reconstructed from showers in the EMC crystals. Each photon is required to have an energy deposition above 25 MeV in the barrel of the EMC ($|\cos\theta| < 0.80$) or 50 MeV in the end caps ($0.86 < |\cos\theta| < 0.92$). To exclude showers due to bremsstrahlung radiation from charged tracks, the angle between the shower position and the nearest charged tracks, extrapolated to the EMC, must be greater than 20 degrees. The timing information from the EMC is restricted to be $0 \leq t \leq 700 \text{ ns}$ to suppress electronic noise and energy deposits unrelated to the event. At least one photon candidate is required.

In order to improve the mass resolution and suppress backgrounds, a one-constraint (1C) kinematic fit is performed under the $e^+e^- \rightarrow \gamma K^\pm K_{\text{miss}}^\mp \ell^+ \ell^-$ hypothesis by constraining the mass of the missing track to be the kaon mass. If there are two kaons or more than one candidate photon, the combination of $\gamma K^\pm K_{\text{miss}}^\mp \ell^+ \ell^-$ with the least χ^2 is accepted. The χ^2 of the kinematic fit is required to be less than 20.

With all of the above selection criteria being applied, the invariant mass distribution of $M(K^+K^-)$ versus $M(\ell^+\ell^-)$ and the corresponding 1-D projections for data are shown in Fig. 1(a-c). By default, M denotes the invariant mass. Obvious signals can be seen in the ϕ and J/ψ mass windows, which are defined as $0.995 \leq M(K^+K^-) \leq 1.048 \text{ GeV}/c^2$ and $3.046 \leq M(\ell^+\ell^-) \leq 3.150 \text{ GeV}/c^2$, respectively. The mass windows of the ϕ and J/ψ are four times the full width at half maximum of the invariant mass distributions of signal events from the MC simulation. The distribution of $M(K^+K^-)$ versus $M(\gamma J/\psi)$ after the J/ψ mass window requirement is shown in Fig. 1(d). The signal regions of χ_{c1} and χ_{c2} states are set to be $[3.49, 3.53]$ and $[3.54, 3.58] \text{ GeV}/c^2$, respectively. Significant accumulations of events can be seen in the intersections of the signal regions.

The same selection criteria are applied to the inclusive MC sample to investigate possible background contributions. No events meet the requirements. Furthermore, exclusive MC samples for several processes, such as $e^+e^- \rightarrow K^+K^-J/\psi$, $\phi\pi^+\pi^-$, $K^+K^-\pi^+\pi^-$, $K^+K^-K^+K^-$, and $K^+K^-\pi^+\pi^-\pi^0$, which are potential background channels but not included in the inclusive MC samples, are generated separately. Each sample contains more than one million events (corresponding to a cross section of 2 nb at the current luminosity). The cross sections of these processes have been measured to be on the order of a few or a few tens of pb [45–48] in the energy range of interest. We find that the dominating background events originate from $e^+e^- \rightarrow K^+K^-J/\psi$ in combination with a photon from initial state radiation. Using the cross section of $e^+e^- \rightarrow K^+K^-J/\psi$ at $\sqrt{s} = 4.600 \text{ GeV}$ measured by BESIII [45], the numbers of background events for the χ_{c1} and χ_{c2} channels normalized to the luminosity of the data sample are estimated to be 0.014 and 0.002, respectively. Simulation studies for all possible backgrounds show that less than 0.2% of the total candidate events are from background contributions.

B. Cross Sections

The distribution of $M(\gamma J/\psi)$ after all event selection requirements is shown in Fig. 2. The χ_{c1} and χ_{c2} signal regions are defined as $[3.49, 3.53]$ and $[3.54, 3.58] \text{ GeV}/c^2$, respectively. 12 and 8 events, respectively, are observed by counting the number of events located in the χ_{c1} and χ_{c2} signal regions.

Assuming that the number of signal and background events both follow a Poisson distribution, the confidence interval $[\mu_a, \mu_b]$ with confidence level $\gamma = 0.6827$, should satisfy the

formulas

$$\int_{\mu=0}^{\mu_a} \sum_{n=0}^N P(n, \mu) \cdot P((N-n), b) d\mu = \frac{1-\gamma}{2} = 0.1587, \quad (1)$$

$$\int_{\mu=0}^{\mu_b} \sum_{n=0}^N P(n, \mu) \cdot P((N-n), b) d\mu = \frac{1+\gamma}{2} = 0.8413, \quad (2)$$

where $P(n, \mu) = \frac{1}{n!} \mu^n e^{-\mu}$ is the probability density function of a Poisson distribution, N is the number of the events observed in the signal region, n is the number of the signal events, μ is the expected number of signal events, b is the expected number of background events, which is estimated using the dedicated background MC samples. The signal yields of the χ_{c1} and χ_{c2} channels are obtained to be $12.0_{-2.6}^{+4.6}$ and $8.0_{-2.0}^{+4.0}$, respectively. The p-value can be obtained by calculating the probability of the expected number of background events to fluctuate to the number of observed events or more in the signal regions assuming a Poisson distribution. The p-value is 1.17×10^{-31} for χ_{c1} and 6.34×10^{-27} for χ_{c2} , corresponding to statistical significances of 11.6σ and 10.6σ , respectively.

The Born cross sections are calculated according to

$$\sigma^B = \frac{N^{\text{sig}}}{\mathcal{L}_{\text{int}} (\epsilon_e \mathcal{B}_e + \epsilon_\mu \mathcal{B}_\mu) \mathcal{B}_{\chi_c} (1+\delta)(1+\delta^{\text{vac}})}, \quad (3)$$

where N^{sig} is the number of the signal events, \mathcal{L}_{int} is the integrated luminosity, ϵ_e and ϵ_μ are the selection efficiencies for the e^+e^- and $\mu^+\mu^-$ modes, respectively, and are listed in Table I, \mathcal{B}_e is the branching fraction $\mathcal{B}(J/\psi \rightarrow e^+e^-)$, \mathcal{B}_μ is the branching fraction $\mathcal{B}(J/\psi \rightarrow \mu^+\mu^-)$, \mathcal{B}_{χ_c} is the branching fraction $\mathcal{B}(\chi_{c1,2} \rightarrow \gamma J/\psi) \mathcal{B}(\phi \rightarrow K^+K^-)$, $(1+\delta)$ is the radiative correction factor, and $(1+\delta^{\text{vac}})$ is the vacuum polarization factor. We assume that the cross section for $e^+e^- \rightarrow \phi \chi_{c1,2}$ follows the $X(4660)$ line shape [10] modified by a two-body phase space factor,

$$BW(\sqrt{s}) = \frac{\Gamma_{ee} \mathcal{B}(\phi \chi_{c1,2}) \Gamma}{(s-M^2)^2 + (M\Gamma)^2} \cdot \frac{\Phi(\sqrt{s})}{\Phi(M)}, \quad (4)$$

where BW is a Breit-Wigner function, the mass (M) and width (Γ) are taken from the Particle Data Group [49], Γ_{ee} is the partial width to e^+e^- , $\mathcal{B}(\phi \chi_{c1,2})$ is the branching fraction of $X(4660) \rightarrow \phi \chi_{c1,2}$, and $\Phi(\sqrt{s}) = \frac{q}{\sqrt{s}}$ is the phase space factor for an S -wave two-body system, where q is the ϕ momentum in the e^+e^- c.m. frame (with $\hbar = c = 1$). The radiative correction factor is obtained with a QED calculation [50], using the Breit-Wigner parameters of $X(4660)$ [10] as input. The vacuum polarization factor $(1+\delta^{\text{vac}}) = 1.055$ is taken from Ref. [51] and its uncertainty is negligible compared with other uncertainties.

The Born cross sections of $e^+e^- \rightarrow \phi \chi_{c1}$ and $\phi \chi_{c2}$ at $\sqrt{s} = 4.600 \text{ GeV}$ are measured to be $4.2_{-1.0}^{+1.7}$ and $6.7_{-1.7}^{+3.4}$ pb, respectively. The numbers used in the calculation and the re-

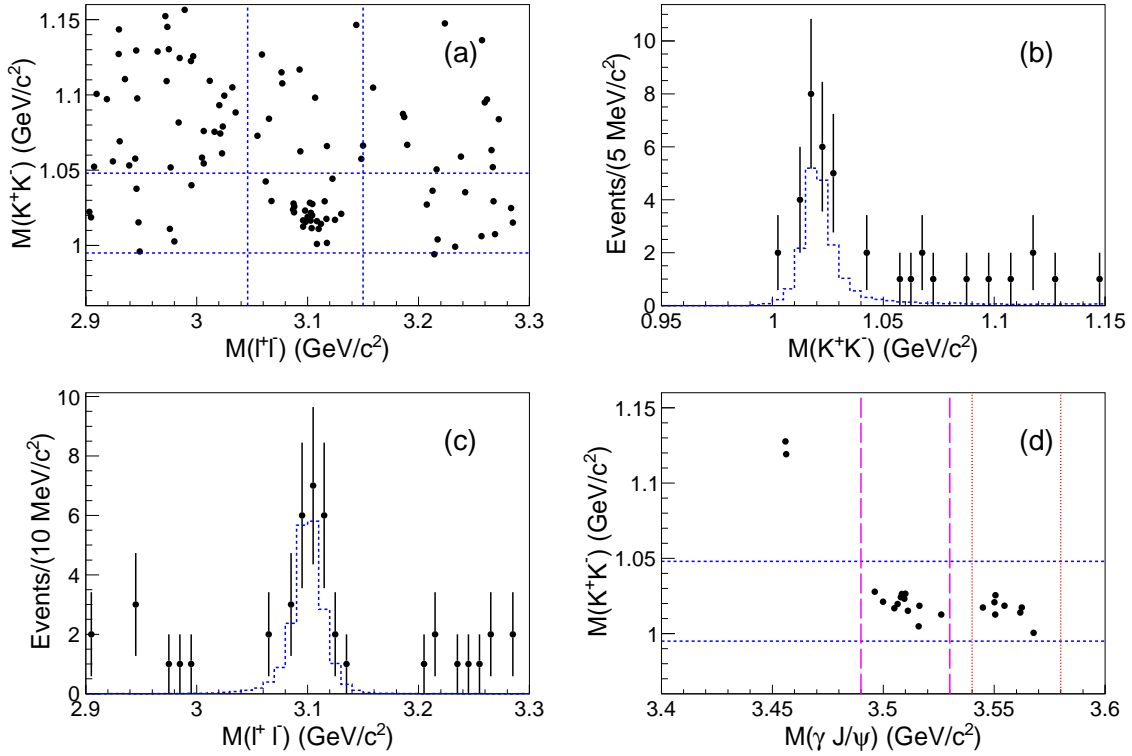


FIG. 1: (Color online) (a) Distribution of $M(K^+K^-)$ versus $M(\ell^+\ell^-)$, (b) the projection along $M(K^+K^-)$ in the J/ψ mass window, (c) the projection along $M(\ell^+\ell^-)$ in the ϕ mass window, and (d) distribution of $M(K^+K^-)$ versus $M(\gamma J/\psi)$ in the J/ψ mass window for data at $\sqrt{s} = 4.600$ GeV. The blue dashed lines represent the mass windows of the ϕ and J/ψ in plot (a) and (d). The blue dashed histograms in (b) and (c) represent the MC simulated shapes of $M(K^+K^-)$ and $M(\ell^+\ell^-)$, respectively, which have been normalized to the measured Born cross sections. The magenta long-dashed and red dotted lines in (d) represent the signal regions of the χ_{c1} and χ_{c2} , respectively.

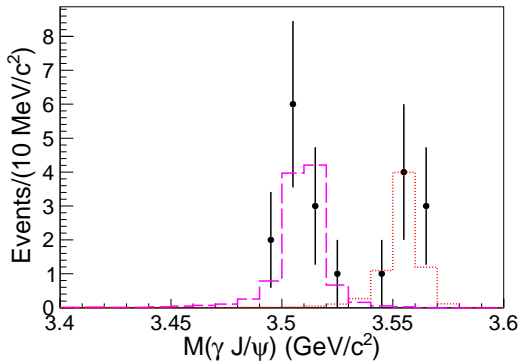


FIG. 2: (Color online) Distribution of $M(\gamma J/\psi)$, after all requirements, for data at $\sqrt{s} = 4.600$ GeV. The markers with error bars are for data. The magenta long-dashed and red dotted histograms are the shapes of the χ_{c1} and χ_{c2} signals from MC simulation, respectively, normalized to the measured Born cross sections.

IV. $e^+e^- \rightarrow \phi\chi_{c0}$

A. Event Selection

1. $\chi_{c0} \rightarrow \pi^+\pi^-/K^+K^-$

For the decay modes $\chi_{c0} \rightarrow \pi^+\pi^-/K^+K^-$, we require that there are three charged particle tracks for which the selection criteria are the same as described above for the $\phi\chi_{c1}$ and $\phi\chi_{c2}$ analyses. Similarly, we require only one kaon from ϕ decays to be reconstructed and pass the PID requirement. The tracks from χ_{c0} decays can be kinematically separated from kaons from ϕ decays, hence the two oppositely charged tracks with momenta greater than 1.0 GeV/ c are assumed to be

TABLE I: The efficiencies (ϵ_e and ϵ_μ), the radiative correction factor ($1 + \delta$), the number of signal events (N^{sig}), the Born cross section (σ^{B}), and the statistical significance for $e^+e^- \rightarrow \phi\chi_{c1}$ and $\phi\chi_{c2}$.

Channel	$\epsilon_e(\epsilon_\mu)(\%)$	$1 + \delta$	N^{sig}	$\sigma^{\text{B}}(\text{pb})$	Significance
$\phi\chi_{c1}$	28.5(38.6)	0.73	$12.0^{+4.6}_{-2.6}$	$4.2^{+1.7}_{-1.0}$	11.6σ
$\phi\chi_{c2}$	21.7(29.6)	0.71	$8.0^{+4.0}_{-2.0}$	$6.7^{+3.4}_{-1.7}$	10.6σ

sults are listed in Table I.

$\pi^+\pi^-$ or K^+K^- pairs from χ_{c0} decays. To separate $\chi_{c0} \rightarrow K^+K^-$ from $\chi_{c0} \rightarrow \pi^+\pi^-$, a 1C kinematic fit is performed with the $e^+e^- \rightarrow K^\pm K_{\text{miss}}^\mp \pi^+\pi^-$ or $K^\pm K_{\text{miss}}^\mp K^+K^-$ hypothesis by constraining the mass of the missing track to the kaon mass. If $\chi^2(\chi_{c0} \rightarrow \pi^+\pi^-) < \chi^2(\chi_{c0} \rightarrow K^+K^-)$, the event is identified as originating from $\chi_{c0} \rightarrow \pi^+\pi^-$, otherwise from $\chi_{c0} \rightarrow K^+K^-$. The χ^2 of the kinematic fit is required to be less than 20. If there is more than one kaon from the ϕ decay identified, the combination with the least χ^2 is retained.

To select signal events, we define the ϕ mass window as four times the full width at half maximum of the distribution of $M(K^+K^-)$ of signal events from the MC simulation, resulting in the requirement that $1.001 \leq M(K^+K^-) \leq 1.038 \text{ GeV}/c^2$. Figure 3 shows the distributions of $M(K^+K^-)$ for low momentum tracks versus $M(\pi^+\pi^-/K^+K^-)$ for high momentum tracks from the data sample, as well as the 1-D projections. No obvious χ_{c0} signals are observed. By studying the inclusive MC sample, we find that more than 90% of background events are from $e^+e^- \rightarrow \phi K^+K^-$.

2. $\chi_{c0} \rightarrow \pi^+\pi^-\pi^+\pi^-$

For the $\chi_{c0} \rightarrow \pi^+\pi^-\pi^+\pi^-$ decay mode, the same event selection criteria for charged tracks are applied. Four pions and only one kaon are required to pass the PID requirement. The total charge of the four pions is required to be zero. In order to improve the mass resolution and suppress backgrounds, a 1C kinematic fit is performed with the $e^+e^- \rightarrow K^\pm K_{\text{miss}}^\mp \pi^+\pi^-\pi^+\pi^-$ hypothesis by constraining the mass of the missing track to the kaon mass. The χ^2 of the kinematic fit is required to be less than 20. If there is more than one kaon, the combination of $K^\pm K_{\text{miss}}^\mp \pi^+\pi^-\pi^+\pi^-$ with the least χ^2 is retained. The ϕ mass window is defined as above to be $0.998 \leq M(K^+K^-) \leq 1.043 \text{ GeV}/c^2$. Figure 4 shows the distribution of $M(K^+K^-)$ versus $M(\pi^+\pi^-\pi^+\pi^-)$ for the data sample and the 1-D projections. Again, there are no obvious χ_{c0} signals.

3. $\chi_{c0} \rightarrow K^+K^-\pi^+\pi^-$

For the $\chi_{c0} \rightarrow K^+K^-\pi^+\pi^-$ decay mode, we use the same criteria to select candidate charged tracks. Two oppositely charged pions and three kaons are required to pass the PID requirement. The absolute value of the net charge of all kaons should not be greater than one. A 1C kinematic fit is performed with the $e^+e^- \rightarrow K^\pm K_{\text{miss}}^\mp K^+K^-\pi^+\pi^-$ hypothesis by constraining the mass of the missing track to the kaon mass and the χ^2 of the kinematic fit is required to be less than 20. If there are more than three kaons, the combination of $K^\pm K_{\text{miss}}^\mp K^+K^-\pi^+\pi^-$ with the least χ^2 is retained. Since the origin of the kaons from ϕ or χ_{c0} decays can not be determined, all combinations of K^+K^- are

considered. The ϕ mass window is defined as above to be $0.998 \leq M(K^+K^-) \leq 1.044 \text{ GeV}/c^2$. The distribution of $M(K^+K^-)$ versus $M(K^+K^-\pi^+\pi^-)$ and the 1-D projections from the data sample are also shown in the Fig. 4. No obvious χ_{c0} signals are observed.

B. Cross Section

A simultaneous unbinned maximum likelihood fit is performed to the distributions of $M(\pi^+\pi^-)$, $M(K^+K^-)$, $M(\pi^+\pi^-\pi^+\pi^-)$, and $M(K^+K^-\pi^+\pi^-)$. The signal shape is determined from the signal MC sample, and the background shape of each decay mode is described with a second-order Chebychev polynomial function. The number of signal events for each decay mode depends on its branching fraction and efficiency. The efficiencies for $\chi_{c0} \rightarrow \pi^+\pi^-$, K^+K^- , $\pi^+\pi^-\pi^+\pi^-$ and $K^+K^-\pi^+\pi^-$ are 62.2%, 58.6%, 29.3%, and 19.7%, respectively. The branching fractions are obtained from the Particle Data Group [49]. Since no significant $\phi\chi_{c0}$ signal is observed, the upper limit on the Born cross section is set at the 90% confidence level (C.L.). A scan of the likelihood with respect to the number of produced $\phi\chi_{c0}$ events is obtained, and the upper limit on n^{prod} at the 90% C.L. is determined according to $\int_0^{n^{\text{prod}}} L(x)dx / \int_0^\infty L(x)dx = 0.9$. Since the branching fractions and efficiencies of the four decay modes have been considered in the fit, the upper limit on the Born cross section is calculated with

$$\sigma^{\text{B}} = \frac{n^{\text{prod}}}{\mathcal{L}_{\text{int}}(1+\delta)(1+\delta^{\text{vac}})}, \quad (5)$$

where $(1+\delta) = 0.74$ [50] and $(1+\delta^{\text{vac}}) = 1.055$ [51] obtained with the same method as for $e^+e^- \rightarrow \phi\chi_{c1,2}$. The upper limit on σ^{B} is obtained by replacing n^{prod} with that on n^{prod} . To take the systematic uncertainty into account, the likelihood distribution is convolved with a Gaussian function with a mean value of 0 and a standard deviation of $n^{\text{prod}} \cdot \Delta$, where n^{prod} is the number of produced $e^+e^- \rightarrow \phi\chi_{c0}$ events and Δ is the relative systematic uncertainty described in next section. The upper limit on the production of $e^+e^- \rightarrow \phi\chi_{c0}$ at the 90% C.L. is estimated to be 5.4 pb.

V. $e^+e^- \rightarrow \gamma X(4140)$

For $e^+e^- \rightarrow \gamma X(4140)$, we search for $X(4140)$ meson decays to $\phi J/\psi$, with J/ψ decaying to $\ell^+\ell^-$, and ϕ decaying to K^+K^- . Since the final state of $e^+e^- \rightarrow \gamma X(4140)$ is the same as that for $e^+e^- \rightarrow \phi\chi_{c1,2}$, we apply the same event selection criteria and requirements. The resulting distributions $M(\phi J/\psi)$ and $M(\gamma J/\psi)$ in the ϕ and J/ψ mass windows are shown in Fig. 5. An unbinned maximum likelihood fit is performed to the distribution of $M(\gamma J/\psi)$. The signal shape is determined from the signal MC sample and the background shapes are described with those from MC simulations for

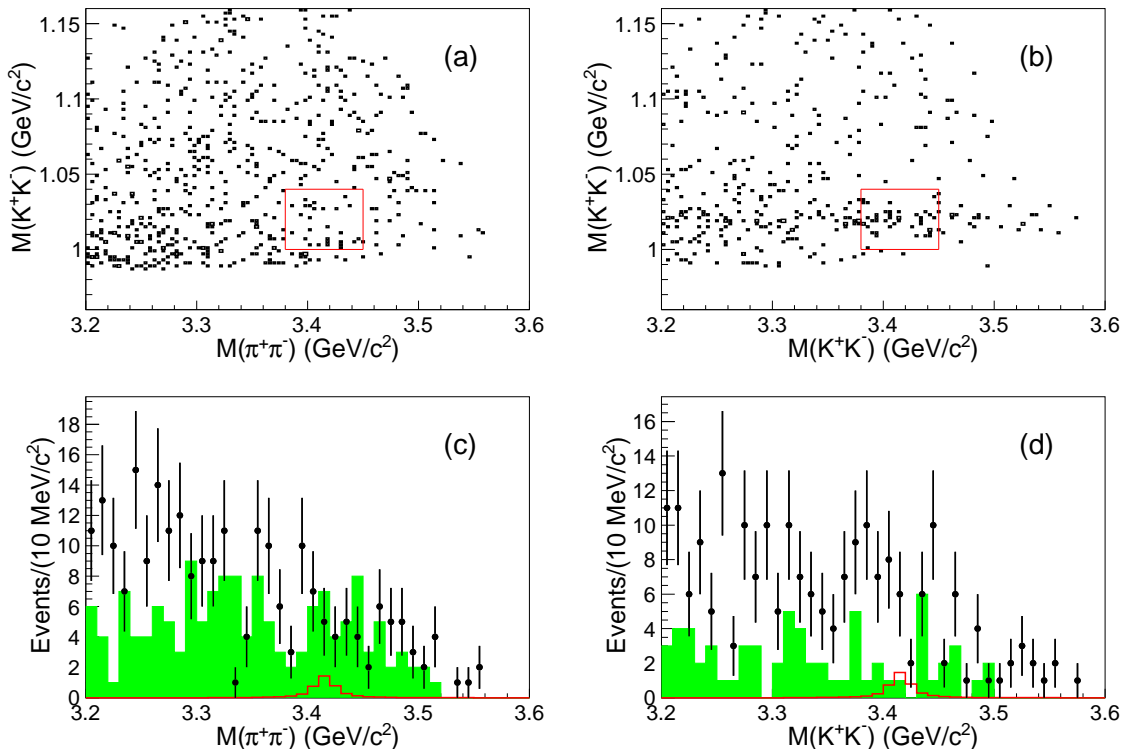


FIG. 3: (Color online) (a, b) Distributions of $M(K^+K^-)$ for low momentum tracks versus $M(\pi^+\pi^-/K^+K^-)$ for high momentum tracks, and (c, d) the projections along $M(\pi^+\pi^-/K^+K^-)$ in the ϕ mass window for the data sample. The red boxes represent the ϕ and χ_{c0} signal regions. The dots with error bars are the data. Histograms filled with green represent the ϕ sidebands, which have been normalized to the signal region of the ϕ . The red histograms represent the χ_{c0} MC shape, normalized to the upper limit of the measured cross section.

$e^+e^- \rightarrow \phi\chi_{c1}$ and $\phi\chi_{c2}$. Since there is no obvious $X(4140)$ signal, the upper limit on the Born cross section at the 90% C.L. is determined. The upper limit on the number of signal events is obtained with the same method as for $e^+e^- \rightarrow \phi\chi_{c0}$. The upper limit on the Born cross section is calculated using Eq. (3), where $(1+\delta) = 0.75$ [50] and $(1+\delta^{\text{vac}}) = 1.055$ [51] obtained with the method described above. The upper limit on the production of the Born cross section and branching fraction $\sigma[e^+e^- \rightarrow \gamma X(4140)] \cdot \mathcal{B}(X(4140) \rightarrow \phi J/\psi)$ at the 90% C.L. is estimated to be 1.2 pb. The distribution of $M(\phi J/\psi)$ is also fitted, but a higher upper limit is obtained. Toy MC samples with the two methods are generated and studied, and we obtain a better sensitivity when applying the fit to $M(\gamma J/\psi)$.

VI. SYSTEMATIC UNCERTAINTY

The systematic uncertainties on the cross section measurements for $e^+e^- \rightarrow \phi\chi_{c0,1,2}$ and $e^+e^- \rightarrow \gamma X(4140)$ come mainly from the integrated luminosity, the tracking and photon reconstruction, the PID, the kinematic fit, the signal and background shapes, the fit range, the branching fraction and the radiative correction. The systematic uncertainties are summarized in Table II and explained below.

The systematic uncertainty due to the detection efficiency includes uncertainties from track reconstruction, PID efficiency, photon reconstruction, the kinematic fit, angular distributions and the radiative correction. The uncertainty from track reconstruction for each charged track is taken as 1.0% [52]. In the process $e^+e^- \rightarrow \phi\chi_{c0}$, the total systematic uncertainty from tracking reconstruction is obtained by taking into account the weights of the efficiencies and branching fractions of the four χ_{c0} decay modes. The total systematic uncertainty due to PID efficiency is obtained with the same method, where the PID uncertainty for each charged track is taken as 1.0% [52]. The systematic uncertainty from photon reconstruction is determined to be 1.0% for each photon by studying the control sample of $J/\psi \rightarrow \rho^0\pi^0$ decays [53].

Since it is difficult to find an appropriate control sample to estimate the systematic uncertainty related to the kinematic fit and the vertex fit, we correct the charged track helix parameters of the MC simulated events [54] to obtain a better match with the data sample. The difference between the efficiency with and without the correction is taken as the uncertainty associated with the kinematic fit. The MC sample with the track helix parameter correction applied is used in the nominal analysis.

In order to estimate the uncertainty from the angular distributions of the ϕ meson and the radiative photon, we change

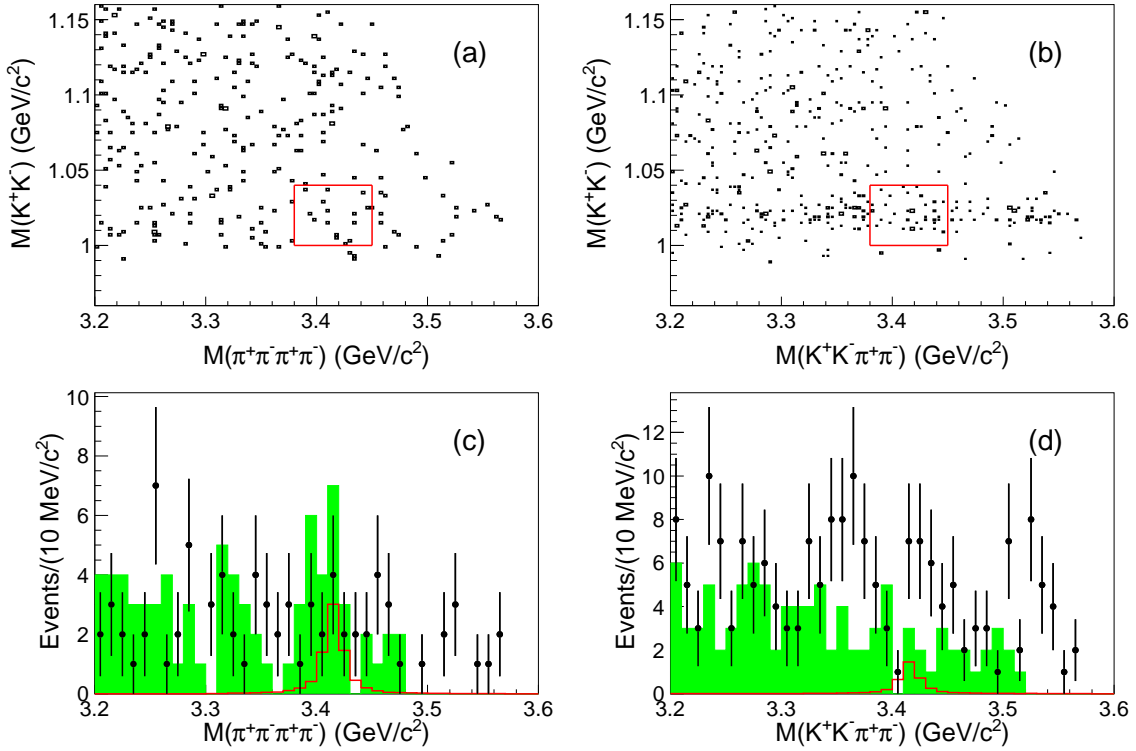


FIG. 4: (Color online) Distributions of (a) $M(K^+K^-)$ versus $M(\pi^+\pi^-\pi^+\pi^-)$, (b) $M(K^+K^-)$ versus $M(K^+K^-\pi^+\pi^-)$, (c) the projection along $M(\pi^+\pi^-\pi^+\pi^-)$ in ϕ mass window, and (d) the projection along $M(K^+K^-\pi^+\pi^-)$ in ϕ mass window for data. The red boxes represent the ϕ and χ_{c0} signal regions. The dots with error bars are the data. The histograms filled with green represent the ϕ sidebands, normalized to the signal region of the ϕ . The red histograms represent the χ_{c0} MC shape, normalized to the upper limit of the measured cross section.

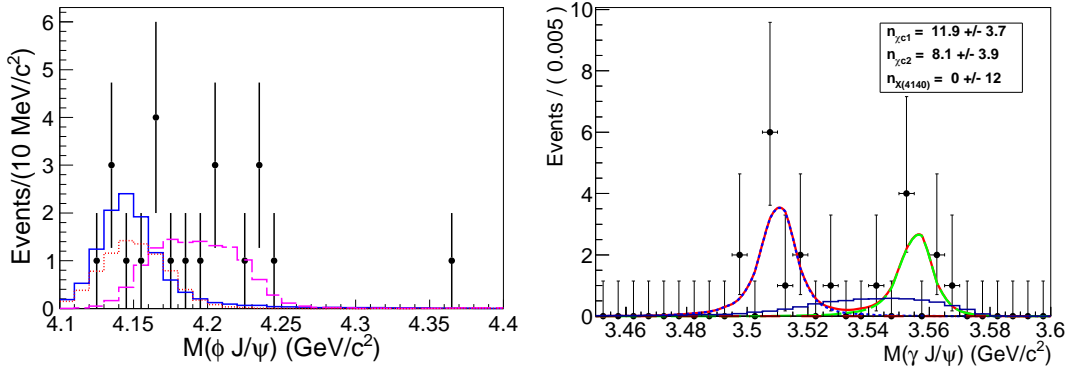


FIG. 5: (Color online) (Left) Distribution of $M(\phi J/\psi)$ in the ϕ and J/ψ mass windows for data. The dots with error bars are the data and the blue solid histogram represents the MC shape from $M(\gamma X(4140))$, normalized to the upper limit of the Born cross section. The magenta long-dashed and red dotted histograms represent the MC shapes from $M(\phi \chi_{c1})$ and $M(\phi \chi_{c2})$, respectively, normalized to the measured Born cross sections. (Right) Fit to the distribution of $M(\gamma J/\psi)$. Dots with error bars are data. Red solid line is the fit curve. Blue dashed and green long-dashed lines represent χ_{c1} and χ_{c2} backgrounds, respectively. Red dash-dotted line represents $X(4140)$ signal. The blue histogram represents the $X(4140)$ signal shape from MC simulation with arbitrary normalization.

the decay dynamics from phase space to $1 + \cos^2 \theta$ or $1 - \cos^2 \theta$ to generate new signal MC samples. For $e^+e^- \rightarrow \gamma X(4140)$, θ is the polar angle of the radiative photon in the e^+e^- rest frame with the z axis pointing in the direction of the electron beam, while for $e^+e^- \rightarrow \phi \chi_{c0,1,2}$, θ is the polar

angle of the ϕ meson. The maximum difference in efficiency is taken as the systematic uncertainty.

The line shape used in the MC simulation will affect both the radiative correction factor and the efficiency. In the nominal MC simulation, we assume that the processes $e^+e^- \rightarrow$

$\phi\chi_{c0,1,2}$ and $e^+e^- \rightarrow \gamma X(4140)$ follow the line shape of the $X(4660)$ [10] modified by a phase space factor. We change the line shape to $\frac{4\pi\alpha^2}{3s}\Phi(\sqrt{s})$ and the resultant difference of $(1 + \delta) \cdot \epsilon$ is taken as the systematic uncertainty due to the radiative correction factor.

The luminosity is measured using large-angle Bhabha events with an uncertainty of less than 1.0% [36]. The branching fractions for $\phi \rightarrow K^+K^-$, $\chi_{c1,2} \rightarrow \gamma J/\psi$, $J/\psi \rightarrow \ell^+\ell^-$ and $\chi_{c0} \rightarrow \pi^+\pi^-$, K^+K^- , $\pi^+\pi^-\pi^+\pi^-$, $K^+K^-\pi^+\pi^-$ are taken from the Particle Data Group [49]. The uncertainties of the branching fractions are taken as the associated systematic uncertainties. For the ϕ and J/ψ mass windows, very loose criteria are used, hence the difference in efficiency between MC simulation and data sample is negligible.

The yields of signal $e^+e^- \rightarrow \phi\chi_{c0}$ and $e^+e^- \rightarrow \gamma X(4140)$ are determined from the fit, and the yields of signal of $e^+e^- \rightarrow \phi\chi_{c1,2}$ is obtained by simply counting events. Only the systematic uncertainty associated with the fit is considered. The systematic uncertainty on the fit procedure comprises those due to the signal shape, background shape and fit range. For $e^+e^- \rightarrow \phi\chi_{c0}$, we generate alternative signal MC samples by varying the mass and width of the χ_{c0} by one standard deviation and take the maximum difference with respect to the nominal values as the systematic uncertainty due to the signal shape. The systematic uncertainty caused by the background shape is obtained by changing the background shape from a second-order polynomial function to a third-order polynomial function. The nominal fit range is taken to be $[3.18, 3.58]$ GeV/ c^2 . We vary the limit of the fit range by ± 0.05 GeV/ c^2 and take the difference as the associated systematic uncertainty. For $e^+e^- \rightarrow \gamma X(4140)$, we generate a signal MC sample by varying the mass and width of the $X(4140)$ with one standard deviation and take the maximum difference as the systematic uncertainty due to the signal shape. The nominal fit range is taken to be $[3.45, 3.60]$ GeV/ c^2 . We vary the limit of the fit range by ± 0.01 GeV/ c^2 and take the resultant difference as the associated systematic uncertainty.

The total systematic uncertainties are obtained by adding the individual uncertainties in quadrature, assuming that all sources are independent. For $e^+e^- \rightarrow \phi\chi_{c0,1,2}$ and $e^+e^- \rightarrow \gamma X(4140)$, the total systematic uncertainties are 12.1%, 7.3%, 7.2% and 19.7%, respectively.

VII. RESULTS AND DISCUSSION

In summary, the processes $e^+e^- \rightarrow \phi\chi_{c1}$ and $\phi\chi_{c2}$ are observed for the first time at a c.m. energy of $\sqrt{s} = 4.600$ GeV by using a data sample corresponding to an integrated luminosity of 567 pb^{-1} collected with the BESIII detector. The corresponding Born cross sections are measured to be

$(4.2_{-1.0}^{+1.7} \pm 0.3) \text{ pb}$ and $(6.7_{-1.7}^{+3.4} \pm 0.5) \text{ pb}$, respectively. No obvious signals are observed for $e^+e^- \rightarrow \phi\chi_{c0}$ and $e^+e^- \rightarrow \gamma X(4140)$ and the upper limits on the Born cross sections at the 90% C.L. are set to be 5.4 pb and 1.2 pb, respectively.

Since only one data set at or near $\sqrt{s} = 4.600$ GeV is available to study these modes at BESIII, it is not possible to measure the line shape for their production. The cross sections of other decay modes at this energy point, such as $e^+e^- \rightarrow \pi^+\pi^- J/\psi$, $e^+e^- \rightarrow \omega\chi_{c0,1,2}$, are all at the level of a few pb. As $e^+e^- \rightarrow \phi\chi_{c1,2}$ signals have been observed, it will be interesting to measure the line shape between the threshold to 4.600 GeV or even higher.

The upper limit of the Born cross section for $e^+e^- \rightarrow \gamma X(4140)$ at 4.600 GeV is higher than those measured at 4.230, 4.260, and 4.360 GeV, due to the non-trivial backgrounds from $\chi_{c1,2}$. Measurements based on data samples with larger statistics at more energy points will be helpful to clarify the nature of these decay processes in this energy region.

Acknowledgments

The BESIII collaboration thanks the staff of BEPCII and the IHEP computing center for their strong support. This work is supported in part by National Key Basic Research Program of China under Contract No. 2015CB856700; National Natural Science Foundation of China (NSFC) under Contracts Nos. 11235011, 11335008, 11425524, 11625523, 11635010; the Chinese Academy of Sciences (CAS) Large-Scale Scientific Facility Program; the CAS Center for Excellence in Particle Physics (CCEPP); Joint Large-Scale Scientific Facility Funds of the NSFC and CAS under Contracts Nos. U1232106, U1332201, U1532257, U1532258; CAS Key Research Program of Frontier Sciences under Contracts Nos. QYZDJ-SSW-SLH003, QYZDJ-SSW-SLH040; 100 Talents Program of CAS; National 1000 Talents Program of China; INPAC and Shanghai Key Laboratory for Particle Physics and Cosmology; German Research Foundation DFG under Contracts Nos. Collaborative Research Center CRC 1044, FOR 2359; Istituto Nazionale di Fisica Nucleare, Italy; Koninklijke Nederlandse Akademie van Wetenschappen (KNAW) under Contract No. 530-4CDP03; Ministry of Development of Turkey under Contract No. DPT2006K-120470; National Science and Technology fund; The Swedish Research Council; U. S. Department of Energy under Contracts Nos. DE-FG02-05ER41374, DE-SC-0010118, DE-SC-0010504, DE-SC-0012069; University of Groningen (RuG) and the Helmholtzzentrum fuer Schwerionenforschung GmbH (GSI), Darmstadt; WCU Program of National Research Foundation of Korea under Contract No. R32-2008-000-10155-0; Shandong Natural Science Funds for Distinguished Young Scholar under Contract No. JQ201402

[1] S. K. Choi *et al.* [Belle Collaboration], ‘‘Observation of a narrow charmoniumlike state in exclusive $B^{+-} \rightarrow$

$K^{+-}\pi^+\pi^- J/\psi$ decays,’’ Phys. Rev. Lett. **91**, 262001 (2003)

- [2] D. Acosta *et al.* [CDF Collaboration], “Observation of the narrow state $X(3872) \rightarrow J/\psi\pi^+\pi^-$ in $p\bar{p}$ collisions at $\sqrt{s} = 1.96$ TeV,” *Phys. Rev. Lett.* **93**, 072001 (2004)
- [3] V. M. Abazov *et al.* [DØ Collaboration], “Observation and properties of the $X(3872)$ decaying to $J/\psi\pi^+\pi^-$ in $p\bar{p}$ collisions at $\sqrt{s} = 1.96$ TeV,” *Phys. Rev. Lett.* **93**, 162002 (2004)
- [4] B. Aubert *et al.* [BABAR Collaboration], “Study of the $B \rightarrow J/\psi K^-\pi^+\pi^-$ decay and measurement of the $B \rightarrow X(3872)K^-$ branching fraction,” *Phys. Rev. D* **71**, 071103 (2005)
- [5] R. Aaij *et al.* [LHCb Collaboration], “Observation of $X(3872)$ production in pp collisions at $\sqrt{s} = 7$ TeV,” *Eur. Phys. J. C* **72**, 1972 (2012)
- [6] B. Aubert *et al.* [BABAR Collaboration], “Observation of a broad structure in the $\pi^+\pi^-J/\psi$ mass spectrum around 4.26 GeV/ c^2 ,” *Phys. Rev. Lett.* **95**, 142001 (2005)
- [7] C. Z. Yuan *et al.* [Belle Collaboration], “Measurement of $e^+e^- \rightarrow \pi^+\pi^-J/\psi$ cross-section via initial state radiation at Belle,” *Phys. Rev. Lett.* **99**, 182004 (2007)
- [8] T. E. Coan *et al.* [CLEO Collaboration], “Charmonium decays of $Y(4260)$, $\psi(4160)$ and $\psi(4040)$,” *Phys. Rev. Lett.* **96**, 162003 (2006)
- [9] B. Aubert *et al.* [BABAR Collaboration], “Evidence of a broad structure at an invariant mass of 4.32 GeV/ c^2 in the reaction $e^+e^- \rightarrow \pi^+\pi^-J/\psi(2S)$ measured at BABAR,” *Phys. Rev. Lett.* **98**, 212001 (2007)
- [10] X. L. Wang *et al.* [Belle Collaboration], “Observation of Two Resonant Structures in $e^+e^- \rightarrow \pi^+\pi^-J/\psi(2S)$ via Initial State Radiation at Belle,” *Phys. Rev. Lett.* **99**, 142002 (2007)
- [11] M. Ablikim *et al.* [BESIII Collaboration], “Observation of a Charged Charmoniumlike Structure in $e^+e^- \rightarrow \pi^+\pi^-J/\psi$ at $\sqrt{s} = 4.26$ GeV,” *Phys. Rev. Lett.* **110**, 252001 (2013)
- [12] M. Ablikim *et al.* [BESIII Collaboration], “Observation of $Z_c(3900)^0$ in $e^+e^- \rightarrow \pi^+\pi^-J/\psi$,” *Phys. Rev. Lett.* **115**, no. 11, 112003 (2015)
- [13] Z. Q. Liu *et al.* [Belle Collaboration], “Study of $e^+e^- \rightarrow \pi^+\pi^-J/\psi$ and Observation of a Charged Charmoniumlike State at Belle,” *Phys. Rev. Lett.* **110**, 252002 (2013)
- [14] T. Xiao *et al.* [CLEO Collaboration], “Observation of the Charged Hadron $Z_c^\pm(3900)$ and Evidence for the Neutral $Z_c^0(3900)$ in $e^+e^- \rightarrow \pi^+\pi^-J/\psi$ at $\sqrt{s} = 4170$ MeV,” *Phys. Lett. B* **727**, 366 (2013)
- [15] M. Ablikim *et al.* [BESIII Collaboration], “Observation of a charged $(D\bar{D}^*)^\pm$ mass peak in $e^+e^- \rightarrow \pi D\bar{D}^*$ at $\sqrt{s} = 4.26$ GeV,” *Phys. Rev. Lett.* **112**, no. 2, 022001 (2014)
- [16] M. Ablikim *et al.* [BESIII Collaboration], “Observation of a Neutral Structure near the $D\bar{D}^*$ Mass Threshold in $e^+e^- \rightarrow (D\bar{D}^*)^0\pi^0$ at $\sqrt{s} = 4.226$ and 4.257 GeV,” *Phys. Rev. Lett.* **115**, no. 22, 222002 (2015)
- [17] M. Ablikim *et al.* [BESIII Collaboration], “Observation of a Charged Charmoniumlike Structure $Z_c(4020)$ and Search for the $Z_c(3900)$ in $e^+e^- \rightarrow \pi^+\pi^-h_c$,” *Phys. Rev. Lett.* **111**, no. 24, 242001 (2013)
- [18] M. Ablikim *et al.* [BESIII Collaboration], “Observation of $e^+e^- \rightarrow \pi^0\pi^0h_c$ and a Neutral Charmoniumlike Structure $Z_c(4020)^0$,” *Phys. Rev. Lett.* **113**, no. 21, 212002 (2014)
- [19] M. Ablikim *et al.* [BESIII Collaboration], “Observation of a charged charmoniumlike structure in $e^+e^- \rightarrow (D^*\bar{D}^*)^\pm\pi^\mp$ at $\sqrt{s} = 4.26$ GeV,” *Phys. Rev. Lett.* **112**, no. 13, 132001 (2014)
- [20] M. Ablikim *et al.* [BESIII Collaboration], “Observation of a neutral charmoniumlike state $Z_c(4025)^0$ in $e^+e^- \rightarrow (D^*\bar{D}^*)^0\pi^0$,” *Phys. Rev. Lett.* **115**, no. 18, 182002 (2015)
- [21] K. Chilikin *et al.* [Belle Collaboration], “Observation of a new charged charmoniumlike state in $B^0 \rightarrow J/\psi K^-\pi^+$ decays,” *Phys. Rev. D* **90**, no. 11, 112009 (2014)
- [22] H. X. Chen, W. Chen, X. Liu and S. L. Zhu, “The hidden-charm pentaquark and tetraquark states,” *Phys. Rept.* **639**, 1 (2016)
- [23] L. Y. Dai, M. Shi, G. Y. Tang and H. Q. Zheng, “Nature of $X(4260)$,” *Phys. Rev. D* **92**, no. 1, 014020 (2015)
- [24] M. Ablikim *et al.* [BESIII Collaboration], “Study of $e^+e^- \rightarrow \omega\chi_{cJ}$ at center-of-mass energies from 4.21 to 4.42 GeV,” *Phys. Rev. Lett.* **114**, no. 9, 092003 (2015)
- [25] M. Ablikim *et al.* [BESIII Collaboration], “Observation of $e^+e^- \rightarrow \omega\chi_{c1,2}$ near $\sqrt{s} = 4.42$ and 4.6 GeV,” *Phys. Rev. D* **93**, no. 1, 011102 (2016)
- [26] M. Ablikim *et al.* [BESIII Collaboration], “Precise measurement of the $e^+e^- \rightarrow \pi^+\pi^-J/\psi$ cross section at center-of-mass energies from 3.77 to 4.60 GeV,” *Phys. Rev. Lett.* **118**, no. 9, 092001 (2017)
- [27] T. Aaltonen *et al.* [CDF Collaboration], “Evidence for a Narrow Near-Threshold Structure in the $J/\psi\phi$ Mass Spectrum in $B^+ \rightarrow J/\psi\phi K^+$ Decays,” *Phys. Rev. Lett.* **102**, 242002 (2009)
- [28] C. P. Shen *et al.* [Belle Collaboration], “Evidence for a new resonance and search for the $Y(4140)$ in the $\gamma\gamma \rightarrow \phi J/\psi$ process,” *Phys. Rev. Lett.* **104**, 112004 (2010)
- [29] J. P. Lees *et al.* [BABAR Collaboration], “Study of $B^{\pm,0} \rightarrow J/\psi K^+K^-K^{\pm,0}$ and search for $B^0 \rightarrow J/\psi\phi$ at BABAR,” *Phys. Rev. D* **91**, no. 1, 012003 (2015)
- [30] S. Chatrchyan *et al.* [CMS Collaboration], “Observation of a peaking structure in the $J/\psi\phi$ mass spectrum from $B^\pm \rightarrow J/\psi\phi K^\pm$ decays,” *Phys. Lett. B* **734**, 261 (2014)
- [31] V. M. Abazov *et al.* [DØ Collaboration], “Search for the $X(4140)$ state in $B^+ \rightarrow J/\psi\phi K^+$ decays with the DØ Detector,” *Phys. Rev. D* **89**, no. 1, 012004 (2014)
- [32] R. Aaij *et al.* [LHCb Collaboration], “Amplitude analysis of $B^+ \rightarrow J/\psi\phi K^+$ decays,” *Phys. Rev. D* **95**, no. 1, 012002 (2017)
- [33] M. Ablikim *et al.* [BESIII Collaboration], “Search for the $Y(4140)$ via $e^+e^- \rightarrow \gamma\phi J/\psi$ at $\sqrt{s} = 4.23, 4.26$ and 4.36 GeV,” *Phys. Rev. D* **91**, no. 3, 032002 (2015)
- [34] M. Ablikim *et al.* [BESIII Collaboration], “Design and Construction of the BESIII Detector,” *Nucl. Instrum. Meth. A* **614**, 345 (2010)
- [35] M. Ablikim *et al.* [BESIII Collaboration], “Measurement of the center-of-mass energies at BESIII via the di-muon process,” *Chin. Phys. C* **40**, no. 6, 063001 (2016)
- [36] M. Ablikim *et al.* [BESIII Collaboration], “Precision measurement of the integrated luminosity of the data taken by BESIII at center of mass energies between 3.810 GeV and 4.600 GeV,” *Chin. Phys. C* **39**, no. 9, 093001 (2015)
- [37] S. Agostinelli *et al.* [GEANT4 Collaboration], “GEANT4: A Simulation toolkit,” *Nucl. Instrum. Meth. A* **506**, 250 (2003)
- [38] Z. Y. Deng *et al.* “Object-Oriented BESIII Detector Simulation System,” *HEP & NP* **30**, 371 (2006)
- [39] S. Jadach, B. F. L. Ward and Z. Was, “Coherent exclusive exponentiation for precision Monte Carlo calculations,” *Phys. Rev. D* **63**, 113009 (2001)
- [40] E. Barberio and Z. Was, “PHOTOS: A Universal Monte Carlo for QED radiative corrections. Version 2.0,” *Comput. Phys. Commun.* **79**, 291 (1994)
- [41] G. Balossini, C. M. Carloni Calame, G. Montagna, O. Nicrosini and F. Piccinini, “Matching perturbative and parton shower corrections to Bhabha process at flavour factories,” *Nucl. Phys. B* **758**, 227 (2006)
- [42] D. J. Lange, “The EvtGen particle decay simulation package,” *Nucl. Instrum. Meth. A* **462**, 152 (2001)
- [43] J. C. Chen, G. S. Huang, X. R. Qi, D. H. Zhang and Y. S. Zhu,

- “Event generator for J/ψ and $\psi(2S)$ decay,” Phys. Rev. D **62**, 034003 (2000)
- [44] T. Sjostrand, L. Lonnblad and S. Mrenna, “PYTHIA 6.2: Physics and manual,” hep-ph/0108264.
- [45] Ke. Li *et al.* [BESIII Collaboration], “New results from $Y(4260)$ decays at BESIII,” XVII International Conference on Hadron Spectroscopy and Structure - Hadron 2017, University of Salamanca, Salamanca, Spain
- [46] T. E. Coan *et al.* [CLEO Collaboration], “Charmonium decays of $Y(4260)$, $\psi(4160)$ and $\psi(4040)$,” Phys. Rev. Lett. **96**, 162003 (2006)
- [47] J. P. Lees *et al.* [BABAR Collaboration], “Cross Sections for the Reactions $e^+e^- \rightarrow K^+K^-\pi^+\pi^-$, $K^+K^-\pi^0\pi^0$, and $K^+K^-K^+K^-$ Measured Using Initial-State Radiation Events,” Phys. Rev. D **86**, 012008 (2012)
- [48] B. Aubert *et al.* [BABAR Collaboration], “The $e^+e^- \rightarrow 2(\pi^+\pi^-)\pi^0$, $2(\pi^+\pi^-)\eta$, $K^+K^-\pi^+\pi^-\pi^0$ and $K^+K^-\pi^+\pi^-\eta$ Cross Sections Measured with Initial-State Radiation,” Phys. Rev. D **76**, 092005 (2007)
- [49] C. Patrignani *et al.* [Particle Data Group], “Review of Particle Physics,” Chin. Phys. C **40**, no. 10, 100001 (2016)
- [50] E. A. Kuraev and V. S. Fadin, “On Radiative Corrections to e^+e^- Single Photon Annihilation at High-Energy,” Sov. J. Nucl. Phys. **41**, 466 (1985)
- [51] S. Actis *et al.* [Working Group on Radiative Corrections and Monte Carlo Generators for Low Energies], “Quest for precision in hadronic cross sections at low energy: Monte Carlo tools vs. experimental data,” Eur. Phys. J. C **66**, 585 (2010)
- [52] M. Ablikim *et al.* [BESIII Collaboration], “Observation of a charged $(D\bar{D}^*)^\pm$ mass peak in $e^+e^- \rightarrow \pi D\bar{D}^*$ at $\sqrt{s} = 4.26$ GeV,” Phys. Rev. Lett. **112**, no. 2, 022001 (2014)
- [53] M. Ablikim *et al.* [BESIII Collaboration], “Branching fraction measurements of χ_{c0} and $\chi_{c2} \rightarrow \pi^0\pi^0$ and $\eta\eta$,” Phys. Rev. D **81**, 052005 (2010)
- [54] M. Ablikim *et al.* [BESIII Collaboration], “Search for hadronic transition $\chi_{cJ} \rightarrow \eta_c\pi^+\pi^-$ and observation of $\chi_{cJ} \rightarrow K\bar{K}\pi\pi$,” Phys. Rev. D **87**, no. 1, 012002 (2013)

TABLE II: The relative systematic uncertainties of Born cross sections (%) for $e^+e^- \rightarrow \phi\chi_{c0,1,2}$ and $e^+e^- \rightarrow \gamma X(4140)$ at $\sqrt{s} = 4.600$ GeV. An ellipsis (\dots) means that the uncertainty is negligible.

Source	$\phi\chi_{c0}$	$\phi\chi_{c1}$	$\phi\chi_{c2}$	$\gamma X(4140)$
Luminosity	1.0	1.0	1.0	1.0
Tracking	4.2	3.0	3.0	3.0
Photon	\dots	1.0	1.0	1.0
PID	3.4	1.0	1.0	1.0
Kinematic fit	1.6	1.5	1.0	2.4
Branching fraction	5.7	3.8	3.9	1.2
Radiative correction	5.2	2.1	2.2	7.3
Angular distribution	3.7	4.5	4.3	13.8
Signal shape	3.4	\dots	\dots	11.0
Background shape	5.2	\dots	\dots	\dots
Fitting range	1.0	\dots	\dots	1.7
Sum	12.1	7.3	7.2	19.7